Magnetic domain pinning in patterned magneto-optical material

Te-Ho Wu
Department of Humanities and Sciences, National Yunlin University of Science and Technology, Touliu, Taiwan 640, Republic of China

J. C. Wu and Y. W. Huang
Department of Physics, National Changhua University of Eduction, Changhua, Taiwan 500, Republic of China

Bing-Mau Chen and Han-Ping D. Schieh
Institute of Electro-Optic Engineering, National Chiao-tung University, Hsinchu, Taiwan 300, Republic of China

Pinning magnetic domains with defined shapes have been made for magneto-optical thin film material. The pinning array of holes on the substrate was fabricated using electron beam lithography. The domain pinning behaviors were studied by applying an external magnetic field perpendicular to the film plane and imaged by atomic force microscopy in their remanent state. Magnetic domains were found to be pinned inside the hole arrays and reproduced the shapes of the holes. The coercivity in the patterned region is larger than in the nonpatterned region. Moreover, the coercivity inside the hole sites is larger than the land sites. © *1999 American Institute of Physics.* [S0021-8979(99)38708-9]

Higher magnetic data storage densities demand smaller stable domains and a reduced media noise. Observations have indicated that some of the media noise arises from domain irregularity, the jagged magnetization transition regions, and a nonuniform distribution of magnetization within recorded domains.[1–3] Consequently, a written domain with fixed shape and free from jaggedness could help reduce the media noise. One way to achieve this goal is by patterning of the disk substrates.[4–8] In this paper, we present a technique for pinning the magnetic domains and study the pinning behaviors by applying an external magnetic field to the samples.

Regular arrays of shaped holes were fabricated using electron-beam lithography. Arrays of square-, circle-, and star-shaped holes were created in the PMMA using a versatile pattern generator.[7,8] The MO active layer $Dy_x(FeCo)_{1-x}$ with 50 nm thickness was dc magnetron cosputtered on to the developed PMMA layer. The layer structure is: silicon/SiN (200 nm)/DyFeCo(50 nm)/SiN(30 nm) in the holes and silicon/SiN (200 nm)/PMMA(x nm)/DyFeCo(50 nm)/SiN(30 nm) on the lands, where x stands for depth of holes (see Fig. 1).

The sample's morphology and magnetic domain structure were observed by employing a magnetic force microscope (MFM). A Digital Instruments Nanoscope IIIa MFM, equipped with a phase extender was used in this study. Before taking the MFM measurements, the samples were either magnetized or demagnetized in magnetic fields perpendicular to the film plane.[9] During the perpendicular demagnetization process a polar Kerr microscope, equipped with an electromagnet of maximum field capability of 8 kOe, was used to monitor the developing magnetic domains.

Domain pinning behaviors were studied on the remanent states after applying a 25 kOe magnetic field perpendicularly to the film plane. Magnetic domains were found to be pinned inside the hole arrays and reproduced the geometric shapes of the holes. Figures 2–3 show the three-dimensional (3D) surface topography images of patterned substrate hole arrays and pinned magnetic domains within hole arrays with different geometric patterns for the $Dy_{22}(Fe_{80}Co_{20})_{78}$ sample. The hole depth for all shapes was 34 nm. Vibrating sample magnetometry (VSM) indicated coercivity of 6.5 kOe and magnetization of 70 emu/cc. Figure 2(a) is a patterned topography of 500-nm-diam circular holes with 1000 nm periods, while Fig. 2(b) shows the corresponding pinned domains within the holes. Figure 3(a) displays the patterned topography of 500 nm×500 nm square holes with a 1000 nm period, while Fig. 3(b) is the corresponding pinned domains within the holes. In order to verify that the frequency shift of Figs. 2(b) and 3(b) really interpreted magnetic signals, an opposite magnetic field (−25 kOe) was applied. The pinned domains showed contrast with the original magnetic moment (not shown). Thus, the frequency shifts of Figs. 2(b) and 3(b) indeed reveal the magnetic domain images.

The cause of the pinning effect is believed to be the total vector effects of both perpendicular magnetizations on the sidewalls and in the bottom areas of the holes. Since the samples we have studied possess perpendicular anisotropy,

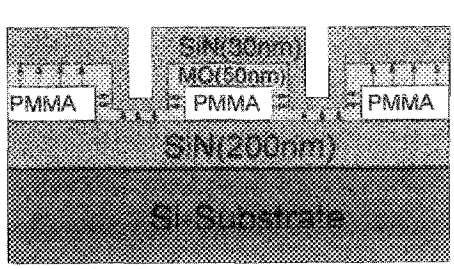

FIG. 1. Schematically displays the layer structure and the magnetization directions of the deposited thin film.

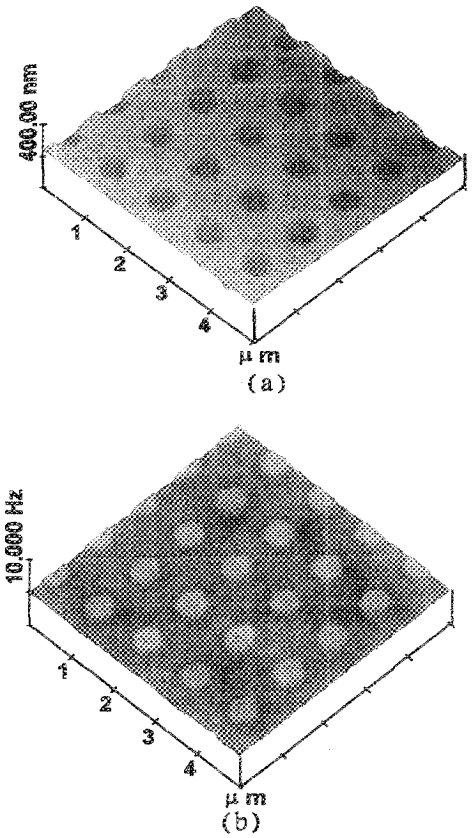

FIG. 2. (a) is a patterned topography of 500-nm-diam circular holes with 1000 nm period; (b) shows the corresponding pinned domains within holes.

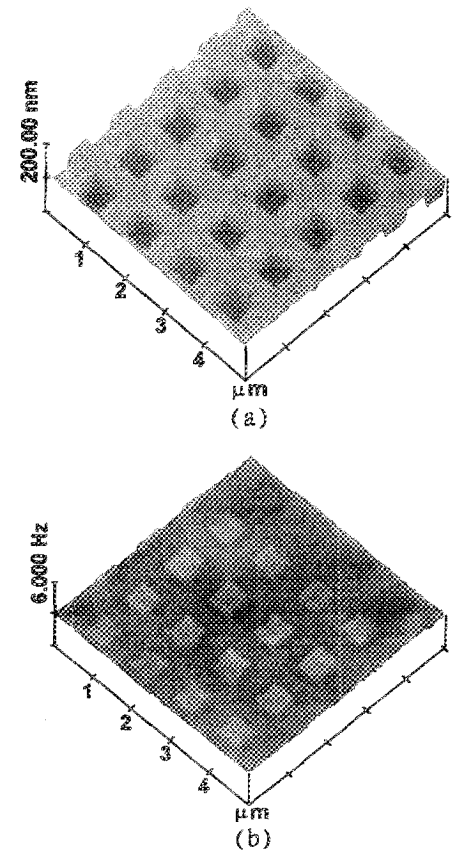

FIG. 3. (a) Displays the patterned topography of 500 nm×500 nm square holes with 1000 nm period; (b) is the corresponding pinned domains within holes.

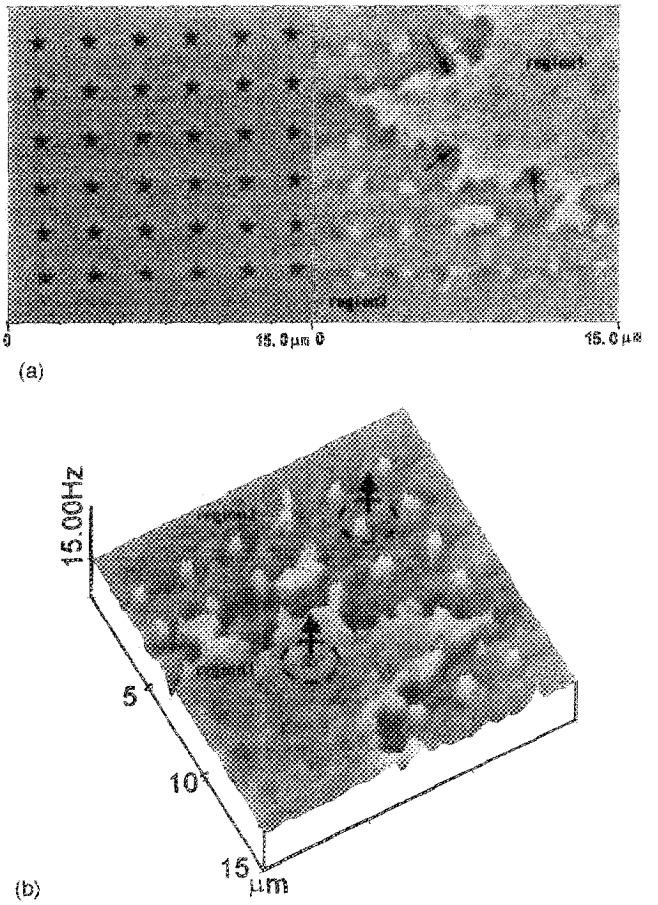

FIG. 4. For the $Dy_{22}(Fe_{80}Co_{20})_{78}$ sample, (a) the left half shows the measured star-shaped topography images; the right half is simultaneously measured magnetic domain image; (b) 3D zoom-in image of right half of (a).

the magnetization direction on every sidewall is almost perpendicular to the magnetization at the bottom. The magnetization near the rim of the hole, instead of being perpendicular, is included towards the surface acting as a transition region and causing the pinning effect.

Another approach in studying the pinning behaviors was accomplished by observing the magnetic domain wall motion across the pinning holes. The experimental results can be best seen from Figs. 4 and 5. Figures 4(a) and 5(a) show star-array topography (left) and magnetic domain images (right) in the demagnetized state for $Dy_{22}(Fe_{80}Co_{20})_{78}$ and $Dy_{27}(Fe_{80}Co_{20})_{73}$ samples, respectively. Figures 4(b) and 5(b) display the 3D magnetic domain zoom-in images of Figs. 4(a) and 5(a), individually. Before comparing the differences between images of Figs. 4 and 5, first of all, we will describe the way in which these images were produced. The magnetic moment of a sample was first saturated in one direction, out-of-plane, by applying a magnetic field much greater than the sample's coercivity. The applied field was then increased in the reverse direction and allowed to approach coercivity, where it caused domain wall creation. As visualized under a Kerr microscope, the domain nucleated outside the patterned area and moved toward the patterned area. When the domain walls moved toward the center of the patterned area, the applied magnetic field was turned off. Pinned magnetic domains were then imaged by MFM. The

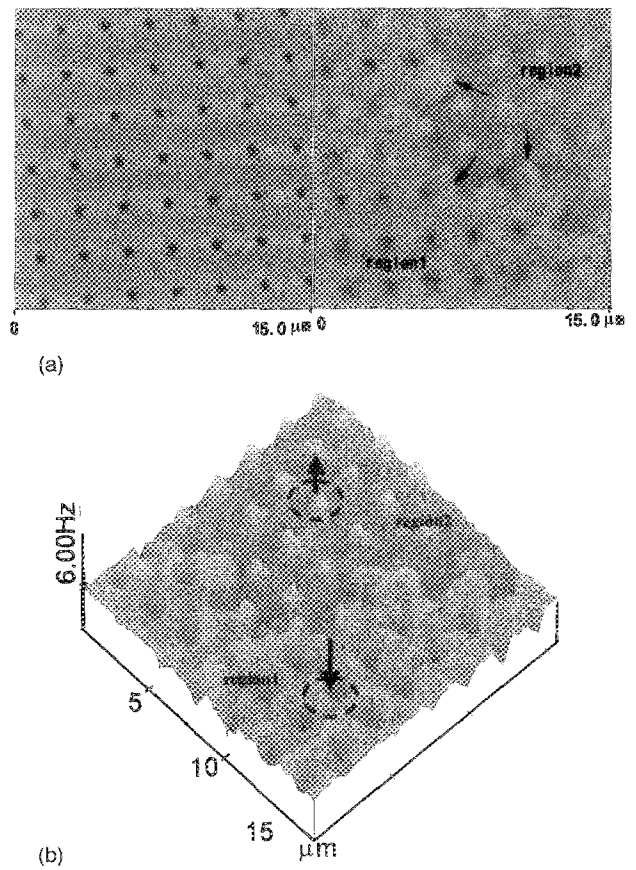

FIG. 5. For the $Dy_{27}(Fe_{80}Co_{20})_{73}$ sample, (a) the left half shows the measured star-shaped topography images; the right half is simultaneously measured magnetic domain image; (b) 3D zoom-in image of right half of (a).

left half of Figs. 4(a) and 5(a) show the measured star-shaped topography images, while, for the same scan area, the right half of Figs. 4(a) and 5(a) are simultaneously measured magnetic domain images with well-defined pinning sites with hole depth of 550 nm in PMMA for $Dy_{22}(Fe_{80}Co_{20})_{78}$ and with hole depth of 300 nm for $Dy_{27}(Fe_{80}Co_{20})_{73}$ samples, respectively. For both images, regions 1 and 2 of the right half represent the opposite magnetic moments of the developed domain; and the arrows indicate the domain wall motion directions as well as the boundary between opposite domains. Careful inspection of the star-shaped pinned domains in region 2 of Figs. 4(a) and 5(a), show the pinning behavior of Fig. 4(a) is quite different from that of Fig. 5(a). In Fig. 5(a), the pinned domains reversed magnetic moment orientation from up-side-down in the area when domain walls moved across the pattern area along the directions as the arrows indicate. On the other hand, in Fig. 4(a), the pinned domains maintained the same moment's orientation after the domain walls moved across the pinning holes. Moreover, the domain wall motion only peeled away the domain in the land area while the enclosed domain of the groove area maintained the same orientation. The different domain pinning manners of Figs. 4(a) and 5(a) can be seen in detail from their 3D zoom-in images, as shown in Figs. 4(b) and 5(b). Figures 4(b) and 5(b) are 3D zoom-in images of right halves of Figs. 4(a) and 5(a), respectively. In Fig. 4(b), both regions 1 and 2 of the star-shaped pinned domains show the same moment's directions, as the dashed-circular enclosed arrows indicate. On the other hand, in Fig. 5(b), the star-shaped pinned domains in region 1 have different directions from region 2, as the dashed-circular enclosed arrows indicate. In addition, we have observed that coercivity in the patterned area is larger than in the outside patterned area; and in the patterned area, the coercivity of holes sites (grooves) is larger or equal to the land sites. Therefore, when the domain wall moves across the patterned area, whether the pinned domains do or do not change the moment orientations, is dependent on the local coercivity strength inside the pinning holes. The coercivity strength with a hole depth of 550 nm is enhanced more than those with a hole depth of 300 nm.

Although we show only circle-, square-, and star-shaped pinning hole arrays, we also made some other shapes, such as donut and concentric circle shapes, to investigate the domain pinning behaviors. They all illustrate pinned domains within hole arrays. Therefore, in principle, it is possible to pin almost any desired magnetic domain geometry with our technique.

This work is supported by the National Science Council, the Republic of China, under Contract No. NSC87-2112-M-224-001.

[1] T.-H. Wu and M. Mansuripur, J. Magn. Soc. Jpn. **17 S1**, 131 (1993).
[2] Y. Honda, N. Inaba, F. Tomiyama, T. Yamamoto, and M. Futamoto, Jpn. J. Appl. Phys., Part 2 **34**, L987 (1995).
[3] C.-J. Lin and D. Rugar, IEEE Trans. Magn. **MAG-24**, 2311 (1988).
[4] S. Gadetsky, T. Suzuki, J. K. Erwin, and M. Mansuripur, J. Magn. Soc. Jpn. **19 S1**, 91 (1995).
[5] S. Y. Chou, M. Wei, P. R. Krauss, and P. B. Fisher, J. Vac. Sci. Technol. B **12**, 3695 (1994).
[6] R. L. White, R. M. H. New, and R. F. W. Pease, IEEE Trans. Magn. **33**, 990 (1997).
[7] T.-H. Wu, J. C. Wu, B. M. Chen, and H. P. D. Shieh, J. Magn. Soc. Jpn. **22 S2**, 145 (1998).
[8] T.-H. Wu, J. C. Wu, B. M. Chen, and H. P. D. Shieh, IEEE Trans. Magn. **34**, 1994 (1998).
[9] T.-H. Wu, J. Appl. Phys. **81**, 5321 (1997).